| INVITED PAPER | *Special Section on Analog Circuits and Related SoC Integration Technologies* |

A Study of Striped Inductor for K- and Ka-Band Voltage-Controlled Oscillators

Nobuyuki ITOH[†a]**,** *Senior Member,* **Hiroki TSUJI**[†]**, Yuka ITANO**[†,††]**,** *Student Members,* **Takayuki MORISHITA**[†]**, Kiyotaka KOMOKU**[†]**,** *Members,* **and Sadayuki YOSHITOMI**[††]**,** *Nonmember*

SUMMARY   A striped inductor and its utilization of a voltage-controlled oscillator (VCO) are studied with the aim of suppressing phase noise degradation in K- and Ka-bands. The proposed striped inductor exhibits reduced series resistance in the high frequency region by increasing the cross-sectional peripheral length, as with the Litz wire, and the VCO of the striped inductor simultaneously exhibits a lower phase noise than that of the conventional inductor. Striped and conventional inductors and VCOs are designed and fabricated, and their use of K- and Ka-bands is measured. Results show that the Q factor and corner frequency of the striped inductor are approximately 1.3 and 1.6 times higher, respectively, than that of the conventional inductor. Moreover, the 1-MHz-offset phase noise of the striped inductor's VCO in the K- and Ka-bands was approximately 3.5 dB lower than that of the conventional inductor. In this study, a 65-nm standard CMOS process was used.
key words: skin effect, striped inductor, Q factor, corner frequency, voltage-controlled oscillator, phase noise

1. Introduction

There have been significant developments in wireless communication since the beginning of this century, and in recent years, connection to the Internet using smart phones, and tablet-PCs has been possible via WLAN or WWAN. Wireless communication is used to not only enable conversation by e-mail or SNS (such as Twitter and Line) but also download huge amount of data in the form of pictures and movies. Therefore, wireless communication demands the availability of high-speed in any place and at any time to enable such downloads. As such a wide signal band-width is essential for enhancing the bit rate of communication [1], and hence, in the case of wireless communication, a high carrier frequency is needed. High operational frequencies of over 20 GHz are therefore of interest, and some applications such as 24 GHz WLAN [2] and IEEE802.11ad [3] have been already launched. In addition, research has also focused on carriers beyond 100 GHz [4].

One of the key blocks in the RF part of wireless transceiver integrated circuits is the voltage-controlled oscillator (VCO) and the performance of VCOs in CMOS integrated circuits has significantly improved over the past 20 years.

Figure 1 shows global conference publication data spanning 20 years (over 320 papers) relating to the dependence of the oscillation frequency on the phase noise of CMOS VCOs at 1-MHz offset from carrier frequency. As shown in Fig. 1, the lowest phase noise of 1-MHz offset from the carrier frequency in each oscillating frequency shows a dependence of approximately 20 dB/dec for the GHz oscillation frequency range.

The relationship between oscillation frequency and phase noise is well known as Leeson's phase noise equation [5], as shown in Eq. (1),

$$L(\varDelta f) = \frac{2kTF}{P_{osc}} \left\{ 1 + \left(\frac{f_{osc}}{2Q_{tank}\varDelta f} \right)^2 \right\} \left(1 + \frac{f_{1/f}}{\varDelta f} \right) \qquad (1)$$

where, $\varDelta f$ is the carrier offset frequency, k is the Boltzmann constant, T is the absolute temperature, F is the noise factor of the gain cell, P_{osc} is the root mean square value of the oscillation power, Q_{tank} is the Q factor of the tank circuit, and $f_{1/f}$ is the flicker noise corner frequency.

As shown in Eq. (1), the theoretical frequency dependence of phase noise at a certain offset frequency should be 20 dB/dec. However, the lowest phase noise beyond K- and Ka-bands does not follow this 20 dB/dec line as shown in Fig. 1, and the possible reasons for this are considered to be among the following: F has been degraded by MOSFET's channel noise enhancement due to scaling [6], $f_{1/f}$ has been degraded by MOSFET's flicker noise enhancement [7], P_{osc} has been degraded by a fall in the power supply due to scaling, or Q_{tank} has been degraded by high frequency operation.
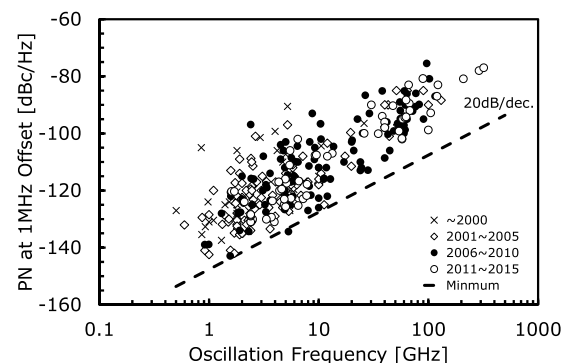

Fig. 1   The global conference publication data spanning 20 years (over 320) relating to the dependence of the oscillation frequency on the phase noise of CMOS VCOs at 1-MHz offset from the carrier frequency.
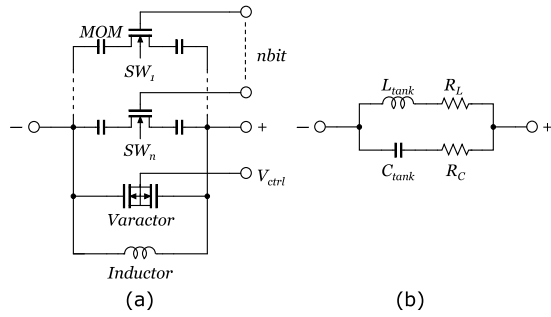
Fig. 2 Typical tank circuit of CMOS LC-VCO (a) and its equivalent circuits (b).

Fig. 3 Overall strategy of our work to improve the Q factor of the tank circuit in the K- and Ka- bands.

In this study, we focus on the cause as the Q factor of the tank circuit degradation beyond K- and Ka-bands.

Figure 2 (a) shows a typical tank circuit using CMOS LC-VCO, which consists of a spiral inductor, a switched capacitor for course tuning, and a varactor for fine tuning; the equivalent circuit is shown in Fig. 2 (b), where, L_{tank}, R_L, C_{tank}, and R_C are the inductance of the tank circuit, the series parasitic resistance of the inductor, the capacitance (which consists of the switched capacitors and the varactor), and the series parasitic resistance of capacitor, respectively.

The Q factors of the inductor, Q_L, capacitor, Q_C, and tank circuit, Q_{tank}, are shown in Eqs. (2) to (4).

$$Q_L = \frac{2\pi f L_{tank}}{R_L} \tag{2}$$

$$Q_C = \frac{1}{2\pi f C_{tank} R_C} \tag{3}$$

$$Q_{tank} = \frac{1}{Q_L^{-1} + Q_C^{-1}} = \frac{2\pi f L_{tank}}{R_L + (2\pi f)^2 L_{tank} C_{tank} R_C} \tag{4}$$

As shown in Eq. (4), Q_{tank} depends on Q_L in the low frequency region but it depends on Q_C in the high frequency region, and therefore a number of researchers have studied ways to improve Q_L below the 10 GHz region [8]–[11]. However, the most serious problem for Q factor degradation in K- and Ka-bands is caused by Q_C degradation. In this respect, we focused on an investigation of Q_C of the varactor, and it was improved sevenfold at $f = 20$ GHz in [12]. This improvement in Q_C provided a significant advantage for improving Q_{tank}. Result, we need improvement of Q_L in the K- and Ka-bands again. Therefore, this study focuses on the improvement of Q_L. Overall strategy of our work is presented in Fig. 3.

This paper is organized as follows. Section 2 describes the skin effect and how to suppress Q factor degradation in the K- and Ka-bands using a striped inductor; Sect. 3 presents the design of the striped inductor and experiments relating to its utilizing of VCO; the measurements and simulation results of inductors and VCOs are shown in Sect. 4; and Sect. 5 concludes the results of this study.
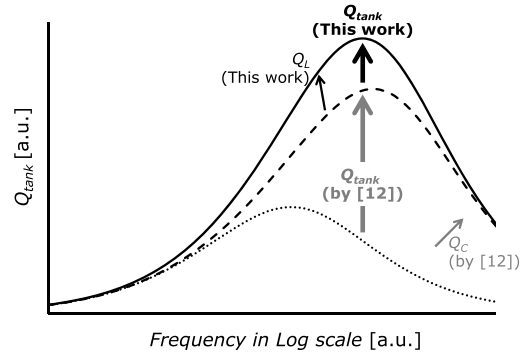
2. Skin Effect in Inductor and Associated Method of Suppression

The skin effect of the spiral inductor occurs in the high-frequency region. The skin depth at a certain frequency, d_s, is defined in Eq. (5) using resistivity, ρ, and permeability, μ of metal [13]. Also, the surface current density, J_S, and the normalized current density at certain depth x, J_X, can be written in Eq. (6).

$$d_S = \sqrt{\frac{\rho}{\pi \mu f}} \tag{5}$$

$$J_X = J_S e^{-\frac{x}{d_S}} \tag{6}$$

The current along the top and the bottom edge of the metal, I_T, and the current along the left and the right edge of the metal, I_W, are possible to be calculated by integrating J_X as shown in Eqs. (7) and (8).

$$I_T = 2 \int_0^{\frac{T}{2}} J_X \, dx = 2 J_S d_S \left(1 - e^{-\frac{T/2}{d_S}}\right) = J_S T_{eff} \tag{7}$$

$$I_W = 2 \int_0^{\frac{W}{2}} J_X \, dx = 2 J_S d_S \left(1 - e^{-\frac{W/2}{d_S}}\right) = J_S W_{eff} \tag{8}$$

where T is the total metal thickness, T_{eff} is the effective metal thickness, W is the total metal width, W_{eff} is the effective metal width of the inductor.

Therefore, T_{eff} and W_{eff}, can be written in Eqs. (9) and (10).

$$W_{eff} = 2 d_S \left(1 - e^{-\frac{W/2}{d_S}}\right) \tag{9}$$

$$T_{eff} = 2 d_S \left(1 - e^{-\frac{T/2}{d_S}}\right) \tag{10}$$

Hence, the effective series resistance, R_{Leff}, of the metal can be written in Eq. (11), where l is the total metal length of the inductor.

$$R_{Leff} = \rho \frac{l}{T_{eff} W + W_{eff} T}$$

$$= \frac{\sqrt{\pi \mu \rho f}}{2} \frac{l}{\left(1 - e^{-\frac{T/2}{d_S}}\right) W + \left(1 - e^{-\frac{W/2}{d_S}}\right) T} \tag{11}$$

In the case of copper wire, the skin depth is less than $0.4\,\mu m$ at the K- and Ka-bands. Therefore, if either the metal width or the metal thickness is larger than $0.8\,\mu m$, the series resistance enlargement by the skin effect occurs, the Q factor of the inductor degrades, and the phase noise of the VCO also significantly degrades.

Equations (12)–(15) define the series resistance of the inductor in the low frequency region, R_{LLF}, that in high frequency region with the skin effect, R_{LHF}, the Q factor of the inductor in the low frequency region, Q_{LLF}, and that in the high frequency region with the skin effect, Q_{LHF}, in the case of W and $T \gg d_s$.

$$R_{LLF} = \rho \frac{l}{WT} \tag{12}$$

$$R_{LHF} = R_{Leff} \approx \sqrt{\pi\mu\rho f}\,\frac{l}{2(W+T)} \quad (W, T \gg d_S) \tag{13}$$

$$Q_{LLF} = \frac{2\pi f L_{tank} WT}{\rho l} \tag{14}$$

$$Q_{LHF} \approx \frac{4\pi f L_{tank} d_S (W+T)}{\rho l} = \frac{4 L_{tank}(W+T)}{l}\sqrt{\frac{\pi f}{\mu\rho}} \tag{15}$$

Equations (12) and (13) show the frequency dependence of the inductor's series resistance. It is evident that although there is zero dependence in the low frequency region, there is a square root dependence in the high frequency region. From this series resistance frequency dependence, the frequency dependence of the Q factor in the low frequency region is of a first order, but that in the high frequency region has a square root. In order to observe whether the skin effect occurs or not, the corner frequency of the skin effect is used as a parameter in Eq. (16).

$$f_C = 4\left(\frac{W+T}{WT}\right)^2 \frac{\rho}{\pi\mu} = \left(\frac{1}{W} + \frac{1}{T}\right)^2 \frac{\rho}{\pi\mu} \tag{16}$$

In the case of skin effect occurrence, the current flow in the inductor is concentrated on the peripheral of the metal line. We thus considered that it may be useful to expand the metal peripheral length to prevent series resistance enhancement due to the skin effect. One of the ideas behind metal peripheral length expansion is enlargement of metal line numbers with keeping total metal width. The 3D-electromagnetic simulation results of current flow in a simple metal line and a striped metal line at $f = 1$MHz and $f = 33$ GHz are shown in Fig. 4. The thickness and the length of all metal line in Fig. 4 are $3.3\,\mu m$ and $200\,\mu m$, and the width of the simple metal line is $7.5\,\mu m$ and the each width of the striped metal line is $2.5\,\mu m$. The material of metal line was assumed copper. The relatively higher current density region is indicated by red and the relatively lower current density region is indicated by blue.

According to Fig. 4 (a) and (b), the current flow at the metal surface is constant for both the simple metal line and the striped metal line in any frequencies, however, the current flow in the metal line at the middle of the metal is not
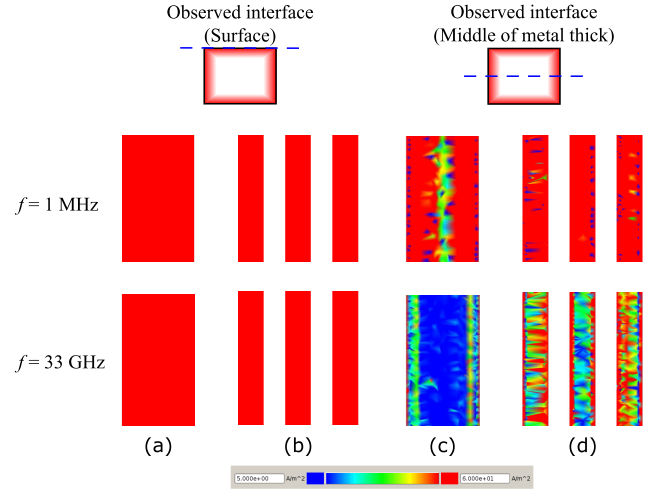

Fig. 4 An observation of the current flow in a simple and a striped metal line at $f = 1$ MHz and $f = 33$ GHz by 3D-electro-magnetic simulation. The simple metal line observed at surface, the striped metal line observed at surface, the simple metal line observed at middle of metal, and the striped metal line observed at middle of metal are shown in (a), (b), (c), and (d), respectively.
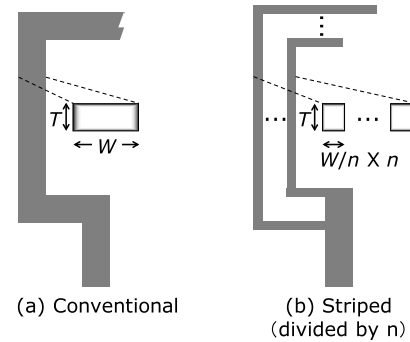

Fig. 5 Basic idea of proposed the striped inductor (b) and the conventional inductor (a).

concentrated in a relatively low frequency region such as $f = 1$MHz, but is concentrated on the peripheral, even when the simple metal or the striped metal line is in a high frequency region such as $f = 33$ GHz, as shown in Fig. 4 (c) and (d). It determined that, in the case of the striped metal line, the current flows on the peripheral of each stripe. Therefore, the total current path of the striped metal line is approximately three times than that of the simple metal line. Also, the current flow of the center of the striped metal line looks relatively low current density than that of the both side of the striped metal line. It seems influence of the proximity effect.

Using this phenomena, we thus proposed the striped inductor shown in Fig. 5 [16]–[20]. In Fig. 5, the conventional and striped inductors are compared. The conventional inductor has one line of metal winding with a width of W, and the striped inductor has n striped metal winding lines each width of W/n, the total metal width of the striped inductor is identical to that of the conventional one. For the current flow

in the case of skin effect occurrence, the conventional inductor has four current paths, bottom, left, top and right which indicates that the peripheral length of the current path is $2W + 2T$, whereas the striped inductor has $4n$ current paths, bottom, left, top and right of each stripe. As the metal width of the striped inductor is already divided by n, the peripheral length of the current flow paths of the striped inductor is thus $2W/n$ (top and bottom of each stripe) $\times n + 2T$ (left and right side of each stripe) $\times n = 2W + 2nT$. This calculation indicates that the striped inductor has $2(n-1)T$ paths more than the conventional inductor, and it is thus considered hopeful that the series resistance of the striped inductor will be lower than that of the conventional one. In addition, it is hoped that the Q factor of the striped inductor will be larger than that of the conventional one.

In consideration of this, the series resistance, Q factor, and corner frequency of the striped inductor, R_{LHFS}, Q_{LHFS}, and f_{CS}, are rewritten as Eqs. (17)–(20), respectively

$$R_{LHFS} = \frac{\sqrt{\pi\mu\rho f}}{2} \frac{l}{\left\{\left(1-e^{-\frac{T/2n}{d_S}}\right)\frac{W}{n}+\left(1-e^{-\frac{W/2n}{d_S}}\right)T\right\}n} \quad (17)$$

$$\approx \sqrt{\pi\mu\rho f}\frac{l}{2(W+nT)} \quad (W, T \gg d_S) \quad (18)$$

$$Q_{LHFS} \approx \frac{4L_{tank}(W+nT)}{l}\sqrt{\frac{\pi f}{\mu\rho}} \quad (19)$$

$$f_{CS} = 4\left(\frac{n}{W}+\frac{1}{T}\right)^2\frac{\rho}{\pi\mu} \quad (20)$$
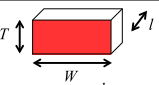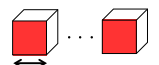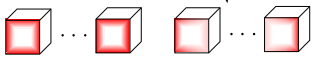
However, in the case of the proximity effect occurrence, the resistance of left and right side current paths of the metal will be large [9], [14], [15]. In this case, n will be smaller than the divide number.

The characterization of the conventional and the striped inductors are summarized in Table 1.

Values of the series resistance of the striped inductor, R_{LHFS}, the Q factor, Q_{LHFS}, and the corner frequency, f_{CS}, can be obtained comparison with those of the conventional inductor according to Eqs. (13) and (18), (15) and (19), and (16) and (20).

$$R_{LHFS} = \frac{W+T}{W+nT}R_{LHF} \quad (21)$$

$$Q_{LHFS} = \frac{W+nT}{W+T}Q_{LHF} \quad (22)$$

$$f_{CS} = \frac{W+nT}{W+T}f_C \quad (23)$$

It is also considered that the following value of the phase noise from the striped inductor's VCO, $L_S(\Delta f)$, may be achieved, in comparison with the VCO of the conventional inductor as shown in Eq. (24).

$$L_S(\Delta f) = \left(\frac{W+T}{W+nT}\right)^2 L(\Delta f) \quad (24)$$

3. Inductor and VCO Design

To validate the performance of the striped inductor and the VCO utilizing it, a discrete inductor test pattern and a VCO test pattern utilizing both the conventional and striped inductors were designed. The details of the inductor are given in Fig. 6.

The conventional inductor designed had a square shape of $D = 50\ \mu$m and it consisted of one metal winding line with $W = 7.5\ \mu$m. On the other hand, the designed striped inductor also had the same square shape ($D = 50\ \mu$m), but it consisted of three metal winding lines with $W = 2.5\ \mu$m, space, $s = 2\ \mu$m. The metal structures of both inductors were M7 (Cu, $T = 3.3\ \mu$m) and M8 (Al, $T = 1.5\ \mu$m) stacked with a lot of vias. The calculated expected values of improvements in series resistance, Q factor and corner frequency of the striped inductor in comparison with the conventional inductor are 0.57, 1.68, and 1.68 times, respectively, using Eqs. (21)–(23).

In addition, three types of VCO pairs are designed to validate the performance of VCOs utilizing the striped inductor. Each pair of VCOs consists of a striped inductor VCO and a conventional inductor VCO. VCO-1 consists of a PMOS gain cell with inductors which shown in Fig. 6, VCO-2 consists of a NMOS gain cell with inductors which shown in Fig. 6, and VCO-3 consists of PMOS gain cell with similar shape inductors which shown in Fig. 6, but its inductor size is $D = 20\ \mu$m. The estimated oscillation frequencies of VCO-1, VCO-2, and VCO-3 were 23, 25, and 40 GHz,

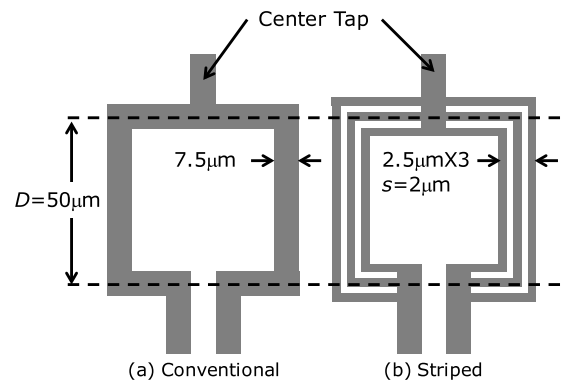**Table 1** Summary of characterization of the conventional and the striped inductors and cross sectional current flow of them.

Fig. 6 Designed conventional inductor (a) and striped inductor (b) for experiments
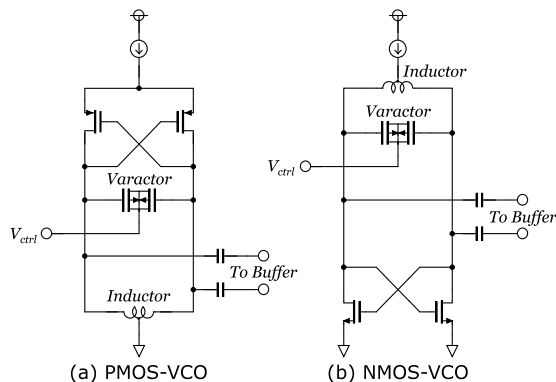
(a) PMOS-VCO (b) NMOS-VCO

Fig. 7 The equivalent circuit of designed PMOS-VCO (a) for VCO-1 and VCO-3, and NMOS-VCO (b) for VCO-2.

Table 2 Summary of designed VCOs.

	Inductor	Gain Cell	fosc [GHz]
VCO-1	D = 50 μm Conventional Striped	PMOS	23
VCO-2	D = 50 μm Conventional Striped	NMOS	25
VCO-3	D = 20 μm Conventional Striped	PMOS	40

(a) Conventional Inductor (b) Striped Inductor

Fig. 8 An observation of the current flow in the conventional and striped inductors at f = 33 GHz by using an electro-magnetic simulator.

Fig. 9 The measured inductance, series resistance, and Q factor of $D = 50\ \mu$m square shaped conventional and those of striped inductor.

respectively. The equivalent circuits of the VCOs are shown in Fig. 7, and the design of the VCO is summarized in Table 2.

The calculated expected value of improvements in phase noise for VCO is 5.0 dB, using Eq. (24).

4. Results and Discussion

In this section, the electro-magnetic simulation result of the discrete inductor, chip measurement results of the discrete inductor, and the chip measurement results of the VCOs are discussed. The test chip fabrication process used in this work is that of Toshiba 65-nm CMOS.

An observation of the current flow in the conventional and striped inductors at $f = 33$ GHz by using an electro-magnetic simulator is shown in Fig. 8, where the electro-magnetic simulator used was EMPro by Keysight Technology Inc. The current flow of both inductors is found to be concentrated in the peripheral of the metal lines. For the conventional inductor, the current flows in both sidewalls of the metal line, and for the striped inductor the current is flowing in both sidewalls of each metal line. Thus, the current paths of the sidewalls of the striped inductor are three times larger than that of the conventional inductor. This result clearly illustrates the usefulness of the striped inductor. However, we were unable to obtain appropriate series resistances of the inductor at high frequency due to difficulties with mesh generation. But we could simulate series resistance at DC, and that of the conventional inductor was
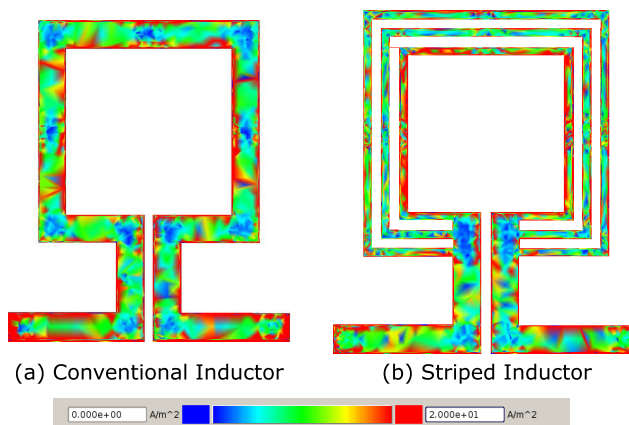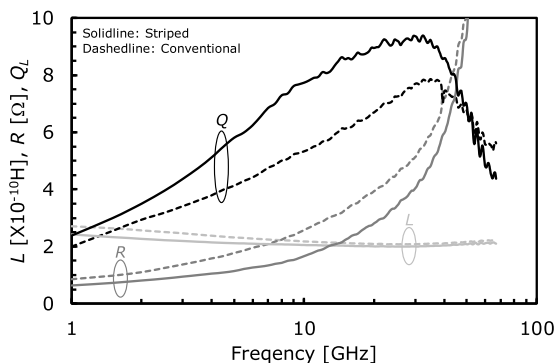
0.18 Ω and that of the striped inductor was 0.17 Ω.

The discrete inductor test chip was measured using a PNA series vector network analyzer from Keysight Technologies Inc. with an on-wafer probe station. The frequency range of the discrete inductor measurement was 1 to 67 GHz. The measured s-parameters were converted into y-parameters, and they were then de-embedded using an open pattern. The inductance, series resistance, and Q factor were extracted from y_{11} [22].

The measured inductance, series resistance, and Q factor of the 50-μm square shaped conventional inductor and the striped inductor are shown in Fig. 9. According to measurement results showed that, both inductors had similar inductance. However, the series resistance of the inductor was entirely different, that of the striped inductor was approximately 0.7, 0.6, and 0.7 times that of the conventional one at $f = 1$, 10, and 25 GHz, respectively. In the case of $f = 1$ to 20 GHz, the measurement value is corresponding to the calculated value, but in the case of $f > 20$ GHz, the measurement value is different a little from the calculated value due to measurement unstableness or unexpected effect for instance the proximity effect. Furthermore, even in $f = 1$ GHz, the skin effect occurs. The calculation value of the series resistance ratio at $f = 1$ GHz using Eqs. (11)

Table 3 Summary of measured inductors.

		D [µm]	W [µm]
Conventional		20	2
			4
		50	2
			4
			7
			7.5
			12
Striped		50	2.5 X 3
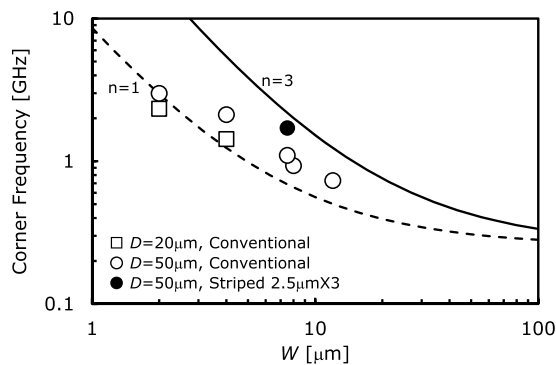
Fig. 10 The experimental results and calculated lines of corner frequencies of one-turn inductors with $T = 4.8$ µm and the calculated lines of corner frequency for $n = 1$ and 3.

and (17) is 0.8. In addition, the Q factor of both inductor was also very different, that of the inductor was approximately 1.5 and 1.3 times larger than conventional one at $f = 15$ GHz and 20 - 25 GHz, respectively. These measurement results show the advantage of using the striped inductor.

The corner frequency was determined using the Q factor vs. frequency data. The merit of the corner frequency evaluation for characterization of the inductor is to eliminate the parasitic resistance influence in measurement, such as contact resistance by the on-wafer probe. Since parasitic resistance does not affect to the corner frequency extraction but it of course affects to the measured series resistance and absolute Q factor. To ensure the data, the corner frequencies of several inductors were determined, as shown in Table 3. The experimental data relating to the metal width dependence of the corner frequency of one-turn inductors, and the calculated lines of corner frequencies are shown in Fig. 10, where $T = 4.8$ µm. Here, open circle denotes the conventional inductor with $D = 50$ µm, open square denotes the conventional inductor with $D = 20$ µm, and closed circle denotes the striped inductor with $D = 50$ µm. Moreover, the solid-and dashed lines denote the calculated corner frequency when $n = 3$ and 1, respectively.

Figure 10 shows that the experimental results and calculated lines of corner frequencies are consistent for both conventional and striped inductors. Furthermore, the cor-

ner frequency of the striped inductor is approximately 1.6 times higher than that of conventional inductor in the case of $W = 7.5$ µm, and as a result, the striped inductor prevents degradation of Q factor of inductor. According to Fig. 10 and Eq. (20), the narrow metal width, the thin metal thickness and the large divide number are essential to obtain high corner frequency. However, the narrow metal width and the thin metal thickness cause higher series resistance as shown in Eq. (18), in other words, Q factor of inductor degrades using the narrow metal or the thin metal. Therefore, large divide number is only solution to obtain high corner frequency and high Q factor.

The VCO test chip was measured using an EXA series signal analyzer by Keysight Technologies Inc. with an on-wafer probe station. The measurement data were corrected at an offset frequency of above 1 MHz to eliminate measured phase noise offset due to AM modulation, because the measurement equipment was not able to cancel this above 1 MHz.

The measured phase noise as a function of the offset frequency from the 23-GHz carrier of the VCO-1 utilizing conventional inductor and the striped inductor are shown in Fig. 11 (a), where the measurement condition was $V_{DD} = 1.2$ V and the core current = 14 mA. The 1-MHz offset phase noise of the striped inductor's VCO was −105.9 dBc/Hz and that of the conventional inductor VCO was −102.3 dBc/Hz. As a result, the 1-MHz offset phase noise of the striped inductor's VCO was exhibited 3.6 dB lower than that of the conventional inductor VCO. By contrast, the estimated improvement of the phase noise of the striped inductor in the thermal noise region was 5.0 dB, as shown in Sect. 3. The cause of difference between the measured value and the estimated value is considered as follows. One is the effective metal of the current flowing is only M7. In that case, calculated phase noise improvement will be 4.1 dB. Another one is influence of the flicker noise up-conversion even at an offset frequency of 1-MHz since the corner frequency of the VCO's flicker noise was approximately 600 kHz which was close from 1 MHz. Moreover, the influence of the proximity effect should be investigated since chip area is limited.

The measured phase noise as a function of the offset frequency from the 25-GHz carrier of the VCO-2 utilizing conventional inductor and the striped inductor are shown in Fig. 11 (b), where the measurement condition was $V_{DD} = 1.2$ V and the core current = 18 mA. The 1-MHz offset phase noise of the striped inductor's VCO was −102.3 dBc/Hz and that of the conventional inductor VCO was −99.8 dBc/Hz. As a result, the 1-MHz offset phase noise of the striped inductor's VCO was exhibited 2.5 dB lower than that of the conventional inductor VCO. In VCO-2, the flicker noise influence was more serious than VCO-1 since the corner frequency of VCO was approximately 1 MHz. Hence, the phase noise improvement of the striped inductor's VCO was compression.

The measured phase noise as a function of the offset frequency from the 40-GHz carrier of the VCO-3 uti-
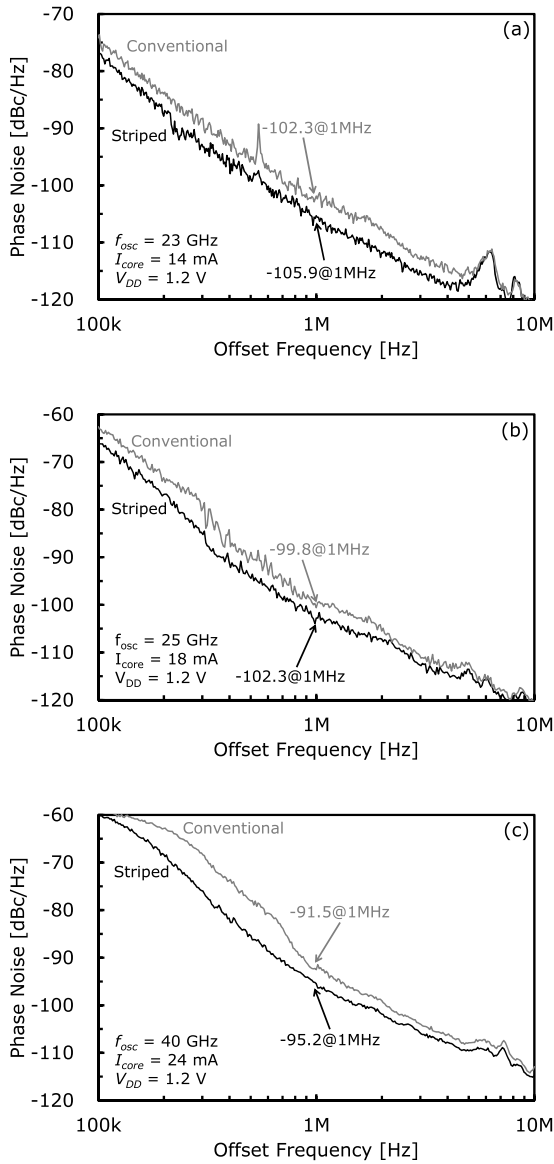
Fig. 11 The measured phase noise of VCO-1 (a), VCO-2 (b), and VCO-3 (c) as a function of the offset frequency from the carrier frequency. The difference of the phase noise between the conventional inductor's VCO and the striped inductor's VCO is exhibited 3.6 dB for VCO-1, 2.5 dB for VCO-2, and 3.7 dB for VCO-3, respectively, at 1-MHz offset from carrier.

Table 4 Summary of measurement data of VCOs.

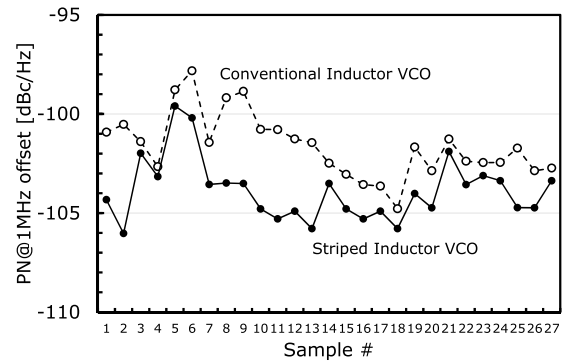|	Inductor	Gain Cell	f_{osc} [GHz]	PN at 1MHz [dBc/Hz]	ΔPN [dB]	P_{DC} [mW]	FOM [dB]
VCO-1	Conv.	PMOS	23	-102.3	3.6	16.8	177.3
	Striped			-105.9			180.9
VCO-2	Conv.	NMOS	25	-99.8	2.5	21.6	174.4
	Striped			-102.3			176.9
VCO-3	Conv.	PMOS	40	-91.5	3.7	28.8	168.9
	Striped			-95.2			172.6
[2]	Conv.	NMOS	24	-110.0	---	22.8	184.0
[20]	Conv.	CMOS	21	-106.0	---	80	173.4

Fig. 12 27 measured samples for the 1-MHz offset phase noise of VCO-1. The closed circles show the phase noise of the striped inductor's VCOs and the open circles show that of the conventional inductor's VCOs.
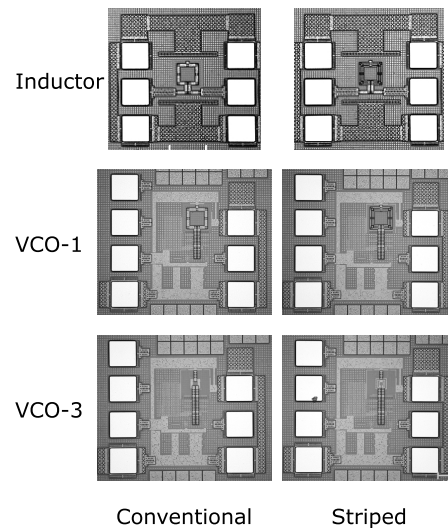
Fig. 13 Chip micro photograph of discrete inductors, VCO-1, and VCO-3 utilized the conventional and striped inductor.

lizing conventional inductor and the striped inductor are shown in Fig. 11 (c), where the measurement condition was V_{DD} = 1.2 V and the core current = 24 mA. The 1-MHz offset phase noise of the striped inductor's VCO was −95.2 dBc/Hz and that of the conventional inductor VCO was −91.5 dBc/Hz. As a result, the 1-MHz offset phase noise of the striped inductor's VCO was exhibited 3.7 dB lower than that of the conventional inductor VCO.

The 1-MHz offset phase noise was improved using the striped inductors for all the VCOs in these experiments in the K- and Ka-band frequency range. However, it is considered that suppression of the flicker noise influence is requires.

$$FOM = \frac{1}{L(\Delta f)}\left(\frac{f_{OSC}}{\Delta f}\right)^2 \frac{1}{P_{DC}}$$

Table 4 compares this study with state-of-the-work K- and Ka-bands VCOs.

Several chips were measured to validate phase noise improvement using the striped inductor. Figure 12 shows

27 measured samples for the 1-MHz offset phase noise of VCO-1, in which the closed circles represent the striped inductor VCOs and open circles those of the conventional inductor. There are variations in the differences between the phase noise of the striped inductor VCOs and that of conventional inductor, but Fig. 12 shows the evident advantage of using the striped inductor.

Figure 13 shows chip micro photographs of the discrete inductors of both the conventional and striped inductor, and that of VCO-1 and VCO-3 utilized the conventional and striped inductor.

5. Conclusion

A striped inductor and its utilization of VCO were studied the aim of suppressing phase noise degradation in K- and Ka-bands. Results showed that the Q factor at f = 25 GHz and the corner frequency of the striped inductor were approximately 1.3 and 1.6 times higher, respectively, than that of the conventional inductor. In addition, the 1-MHz-offset phase noise of the VCO of the striped inductor in K- and Ka-bands approximately 3.5 dB lower than that of the conventional inductor. These results indicate that the proposed striped inductor exhibited reduced series resistance in the high frequency region by preventing the skin effect. However, it is evident that future studies are required to investigate the current flowing paths in the case of the stacked metal and the influence of the proximity effect. In this study, 65-nm standard CMOS process was used.

Acknowledgments

References

[1] C.E. Shannon, "A Mathematical Theory of Communication," The Bell System Technical Journal, vol.27, no.3, pp.379–423, July 1948.

[2] A. Mazzanti, M. Sosio, M. Repossi, and F. Svelto, "A 24GHz subharmonic receiver front-end with integrated multi-phase LO generation in 65nm CMOS," ISSCC 2008, vol.51, pp.216–217, Feb. 2008.

[3] K. Okada, K. Kondou, M. Miyahara, M. Shinagawa, H. Asada, R. Minami, T. Yamaguchi, A. Musa, Y. Tsukui, Y. Asakura, S. Tamonoki, H. Yamagishi, Y. Hino, T. Sato, H. Sakaguchi, N. Shimasaki, T. Ito, Y. Takeuchi, N. Li, Q. Bu, R. Murakami, K. Bunsen, K. Matsushita, M. Noda, and A. Matsuzawa, "Full Four-Channel 6.3-Gb/s 60-GHz CMOS Transceiver with Low-Power Analog and Digital Baseband Circuitry," IEEE J. Solid-State Circuits, vol.48, no.1, pp.46–65, Jan. 2013.

[4] K. Katayama, M. Motoyoshi, K. Takano, N. Ono, and M. Fujishima, "28mW 10Gbps Transmitter for 120GHz ASK Transceiver," IMS, pp.1–3, June 2012.

[5] D.B. Leeson, "A simple model of feedback oscillator noise spectrum," Proc. IEEE, vol.54, no.2, pp.329–330, Feb. 1966.

[6] N. Itoh, K. Kojima, and T. Ohguro, "Channel Noise Enhancement in Small Geometry MOSEFT and Its Influence on Phase Noise Calculation of Integrated Voltage-Controlled-Oscillator," International Journal of Numerical Modelling, vol.18, no.4, pp.255–266, John Wiley & Sons, July 2005.

[7] H. Kimijima, T. Ohguro, B. Evans, B. Acker, J. Bloom, H. Mabuchi, K. Dim-Lee, E. Morifui, T. Yoshitomi, H.S. Momose, M. Kinugawa, Y. Katsumata, and H. Iwai, "Improvement of 1/f noise by using VHP (Vertical High Pressure) oxynitridegate insulator for deep-sub micron RF and analog CMOS," Symp. VLSI Tech. Dig., pp.119–120, Kyoto, 1999.

[8] C.P. Yue and S.S. Wong, "Physical Modeling of Spiral Inductors on Silicon," IEEE Trans. Electron Devices, vol.47, no.3, pp.560–568, March 2000.

[9] Y. Cao, R.A. Groves, X. Huang, N.D. Zamdmer, J.-O. Plouchart, R.A. Wachnik, T.-J. King, and C. Hu, "Frequency-Independent Equivalent-Circuit Model for On-Chip Spiral Inductors," IEEE J. Solid-State Circuits, vol.38, no.3, pp.419–426, March 2003.

[10] C.B. Sia, K.S. Yeo, M.A. Do, and J.-G. Ma, "Metallization Proximity Studies for Copper Spiral Inductors on Silicon," IEEE Trans. Semicond. Manuf., vol.16, no.2, pp.220–227, May 2003.

[11] J.M. Lopez-Villegas, J. Samitier, C. Cane, P. Losantos, and J. Bausells, "Improvement of the Quality Factor of RF Integrated Inductors by Layout Optimization," IEEE Trans. Microw. Theory Techn., vol.48, no.1, pp.76–83, Jan. 2000.

[12] Y. Itano, S. Morimoto, S. Yoshitomi, and N. Itoh, "High-Q MOS Varactor Models for Quasi-Millimeter-Wave Low-Noise LC-VCOs," IEICE Trans. Fundamentals, vol.E97-A, no.3, pp.759–767, March 2014.

[13] F.W. Grover, Inductance Calculations, Dover Publications, ISBN-13:978-0-486-47440-3, 1946.

[14] R.-J. Chan and J.-C. Guo, "Analysis and Modeling of Skin and Proximity Effects for Millimeter-Wave Inductors Design in Nanoscale Si CMOS," Proc. 9th European Microwave Integrated Circuits Conference, pp.13–16, Oct. 2014.

[15] X. Nan and C.R. Sullivan, "An Improved Calculation of Proximity-Effect Loss in High-Frequency Windings of Round Conductors," IEEE 34th Annual Power Electronics Specialist Conference, vol.2, pp.853–860, June 2003.

[16] N. Itoh, Y. Itano, S. Morimoto, and S. Yoshitomi, "Striped Inductor for Quasi Millimeter Wave Voltage-Controlled Oscillator," Proc. Asia-Pacific Microwave Conference, pp.319–321, Seoul, Nov. 2013.

[17] H. Tsuji, Y. Itano, K. Komoku, T. Morishita, S. Yoshitomi, and N. Itoh, "Millimeter-Wave VCO using Striped Inductor," Proc. Asia-Pacific Microwave Conference 2014, pp.959–961, Sendai, Nov. 2014.

[18] N. Itoh, Y. Itano, H. Tsuji, K. Komoku, T. Morishita, and S. Yoshitomi, "A Study of enhancement of Q-factor of LC Resonators in high frequency region," IEICE Technical Report, ICD2014-24, July 2014.

[19] N. Itoh, H. Tsuji, Y. Itano, K. Komoku, T. Morishita, and S. Yoshitomi, "A Study of High-Frequency Characteristics of Stripe Shaped Inductor and its Application for Voltage-Controlled Oscillator," IEICE Technical Report, EMCJ2015-74, MW2015-113, EST2015-84, Oct. 2015.

[20] H. Tsuji, Y. Itano, K. Komoku, T. Morishita, S. Yoshitomi, and N. Itoh, "A Study of Flicker Noise Suppression of K-Band VCO using Striped Inductor," Proc. Asia-Pacific Microwave Conference 2015, WE4E-1, Nanjing, Dec. 2015.

[21] O. Richard, A. Siligaris, F. Badets, C. Dehos, C. Dufis, P. Busson, P. Vincent, D. Belot, and P. Urard, "A 17.5-to-20.94GHz and 35-to-41.88GHz PLL in 65nm CMOS for Wireless HD Applications," ISSCC 2010, vol.53, pp.252–253, Feb. 2010.

[22] S. Yoshitomi, "Analysis and simulation of spiral inductor fabricated on silicon substrate," Proc. 2004 11th IEEE International Conference on Electronics, Circuits and Systems, pp.365–368, Dec. 2004.

Nobuyuki Itoh received the B.S. and M.S. degrees in chemistry from Tokyo University of Science, Tokyo, Japan, in 1983 and 1985 respectively, and the Ph.D. degree in physical electronics from Tokyo Institute of Technology, Tokyo, Japan, in 2006. In 1985, he joined the Research and Development Center, Toshiba Corporation, Kawasaki, Japan, where he was engaged in the research and development of CMOS device technologies, bipolar device technologies, bipolar circuits design and RFCMOS circuit design. He had been a Visiting Scientist at Katholieke Universiteit Leuven, ESAT-MICAS, Leuven, Belgium, from 1996 to 1998, where he had worked on design of fully integrated VCOs and PLLs using RFCMOS. He has been engaged in the research and development of high-frequency analog circuit at Semiconductor Company of Toshiba Corporation since 1998. He was also a part-time lecturer of Chuo University, Tokyo, Japan, since 2009. Since 2010, he has been full time professor of Okayama Prefectural University. His current research interests are high-frequency integrated circuit for telecommunications. Dr. Itoh is a member of IEEE and also senior member of IEICE. He received the Asia-Pacific Microwave Conference (APMC) Prize in 2007. He has been a member of TPC of CICC, BCTM, ESSCIRC, TJMW, and RFIC symposium, was a secretary of IEEE MTT-S Japan Chapter, was the Publicity Chair of APMC 2010, and was a secretary of URSI-C Japan Committee.

Hiroki Tsuji received the B.E. degree from Okayama Prefectural University, Soja, Japan, in 2014. He is currently pursuing M.E. at Okayama Prefectural University, Soja, Japan. His current research interests are high-frequency integrated circuit for telecommunications.

Yuka Itano received the B.S. and M.S degrees in physics from Nara Women's University, Nara, Japan in 2006 and 2008, respectively. In 2008, she joined Semiconductor Mass Storage Company, Toshiba Corporation, Kawasaki, Japan, where she was engaged in Analog Device Design Engineering Group Analog & Imaging Sensor Division. She is currently pursuing Ph.D. at Okayama Prefectural University, Soja, Japan.

Takayuki Morishita received the B.S., M.S. and Ph.D. degrees in electronics from Okayama University, Okayama, Japan, in 1979, 1981 and 1988, respectively. In April 1993, he joined the Department of Communication Engineering at Okayama Prefectural University, as an associate professor. His current research interests are reconfigurable microprocessors and VLSI design.

Kiyotaka Komoku received the B.S. and M.S. degrees in Physics from Okayama University, Okayama, Japan, in 1991 and 1994, respectively. In 1994, he joined the Department of Communication Engineering at Okayama Prefectural University, Okayama, Japan, and is presently an assistant professor. His research interests are media processing using reconfigurable device and VLSI design.

Sadayuki Yoshitomi received the B.E. and M.E, and Ph.D. degrees from Yokohama National University, Yokohama, Japan, 1988, 1990, and 1993, respectively. His title of his doctor thesis was "The study on the silicon dioxide film deposited by liquid phase deposition (LPD)". His background is the physics of Si/SiO2 interface. In 1993, he joined the Research and Development Center, Toshiba Corporation, Kawasaki, Japan, where he is currently engaged in the development of design infrastructures of analog and RF CMOS and BiCMOS process technology. He has been a member of TPC of MIXDES, and an organizing committee of MOS-AK/GSA (Global Semiconductor Alliance).